Draft version August 2, 2024
Typeset using LaTeX twocolumn style in AASTeX631

Discovery of Polarized X-Ray Emission from the Accreting Millisecond Pulsar SRGA J144459.2−604207

Alessandro Papitto,[1] Alessandro Di Marco,[2] Juri Poutanen,[3,4] Tuomo Salmi,[5,6] Giulia Illiano,[1,7,8] Fabio La Monaca,[2] Filippo Ambrosino,[1] Anna Bobrikova,[3] Maria Cristina Baglio,[9] Caterina Ballocco,[1,8] Luciano Burderi,[10,11] Sergio Campana,[9] Francesco Coti Zelati,[12,13] Tiziana Di Salvo,[14] Riccardo La Placa,[1] Vladislav Loktev,[3] Sinan Long,[15] Christian Malacaria,[1] Arianna Miraval Zanon,[16] Mason Ng,[17] Maura Pilia,[18] Andrea Sanna,[11] Luigi Stella,[1] Tod Strohmayer,[19,20] and Silvia Zane[15]

[1] *INAF Osservatorio Astronomico di Roma, Via Frascati 33, 00078 Monte Porzio Catone (RM), Italy*
[2] *INAF Istituto di Astrofisica e Planetologia Spaziali, Via del Fosso del Cavaliere 100, 00133 Roma, Italy*
[3] *Department of Physics and Astronomy, 20014 University of Turku, Finland*
[4] *Space Research Institute, Russian Academy of Sciences, Profsoyuznaya 84/32, 117997 Moscow, Russia*
[5] *Anton Pannekoek Institute for Astronomy, University of Amsterdam, Science Park 904, 1098XH Amsterdam, the Netherlands*
[6] *Department of Physics, P.O. Box 64, 00014 University of Helsinki, Finland*
[7] *Tor Vergata University of Rome, Via della Ricerca Scientifica 1, 00133 Roma, Italy*
[8] *Sapienza Università di Roma, Piazzale Aldo Moro 5, 00185 Rome, Italy*
[9] *INAF Osservatorio Astronomico di Brera, Via E. Bianchi 46, 23807 Merate (LC), Italia*
[10] *INAF/IASF Palermo, Via Ugo La Malfa 153, 90146 Palermo, Italy*
[11] *Dipartimento di Fisica, Università degli Studi di Cagliari, SP Monserrato-Sestu, KM 0.7, Monserrato 09042, Italy*
[12] *Institute of Space Sciences (ICE, CSIC), Campus UAB, Carrer de Can Magrans s/n, 08193 Barcelona, Spain*
[13] *Institut d'Estudis Espacials de Catalunya (IEEC), 08860 Castelldefels (Barcelona), Spain*
[14] *Dipartimento di Fisica e Chimica – Emilio Segrè, Università di Palermo, Via Archirafi 36, 90123 Palermo, Italy*
[15] *Mullard Space Science Laboratory, University College London, Holmbury St Mary, Dorking, Surrey RH5 6NT, UK*
[16] *ASI - Agenzia Spaziale Italiana, Via del Politecnico snc, 00133 Rome (RM), Italy*
[17] *MIT Kavli Institute for Astrophysics and Space Research, Massachusetts Institute of Technology, Cambridge, MA 02139, USA*
[18] *INAF Osservatorio Astronomico di Cagliari, Via della Scienza 5, 09047 Selargius (CA), Italy*
[19] *Astrophysics Science Division, NASA Goddard Space Flight Center, Greenbelt, MD 20771, USA*
[20] *Joint Space-Science Institute, NASA Goddard Space Flight Center, Greenbelt, MD 20771, USA*

(Received August 2, 2024; Revised; Accepted)

Submitted to ApJL

ABSTRACT

We report on the discovery of polarized X-ray emission from an accreting millisecond pulsar. During a 10 day-long coverage of the February 2024 outburst of SRGA J144459.2−604207, the Imaging X-ray Polarimetry Explorer (IXPE) detected an average polarization degree of the 2–8 keV emission of $2.3\% \pm 0.4\%$ at an angle of $59^\circ \pm 6^\circ$ (East of North; uncertainties quoted at the 1σ confidence level). The polarized signal shows a significant energy dependence with a degree of $4.0\% \pm 0.5\%$ between 3 and 6 keV and $< 2\%$ (90% c.l.) in the 2–3 keV range. We used NICER, XMM-Newton, and NuSTAR observations to obtain an accurate pulse timing solution and perform a phase-resolved polarimetric analysis of IXPE data. We did not detect any significant variability of the Stokes parameters Q and U with the spin and the orbital phases. We used the relativistic rotating vector model to show that a moderately fan-beam emission from two point-like spots at a small magnetic obliquity ($\simeq 10^\circ$) is compatible with the observed pulse profile and polarization properties. IXPE also detected 52 type-I X-ray bursts, with a recurrence time $\Delta t_{\rm rec}$ increasing from 2 to 8 h as a function of the observed count rate C as $\Delta t_{\rm rec} \propto C^{-0.8}$. We stacked the emission observed during all the bursts and obtained an upper limit on the polarization degree of 8.5% (90% c.l.).

Corresponding author: Alessandro Papitto
alessandro.papitto@inaf.it

Keywords: magnetic fields – methods: observational – polarization – pulsars: individual: SRGA J144459.2−604207 – stars: neutron – X-rays: binaries

1. INTRODUCTION

The simultaneous measurement of the mass M and the equatorial radius $R_{\rm eq}$ of a few neutron stars (NSs) is of paramount importance for constraining the equation of state of ultra-dense matter because of its one-to-one mapping to the NS mass–radius dependence (Lattimer & Prakash 2016; Özel & Freire 2016; Baym et al. 2018). Relativistic effects bend the light trajectory and modify energy of the photons emitted by hot spots on the surface of millisecond pulsars (MSPs; see, e.g., Watts et al. 2016, and references therein). As a result, modeling the X-ray pulse profiles of MSPs is one of the most powerful techniques to obtain the desired information on M and $R_{\rm eq}$ (Poutanen & Gierliński 2003; Miller & Lamb 2016). The pulse shape also depends on several geometrical parameters (e.g., the binary inclination i, the spot colatitude θ, and its angular size ρ) as well as spectral parameters (e.g., the angular pattern of the emitted radiation; see, e.g., Fig. 1 of Poutanen & Beloborodov 2006 for the geometry assumed). Breaking this degeneracy with X-ray spectral-timing data requires a very large number of counts (Lo et al. 2013; Miller & Lamb 2015). A few megasecond-long NICER observations of rotation-powered MSPs met this requirement and led to constraints on M and $R_{\rm eq}$ with a relative uncertainty of $\sim$ 10% for three of them (Riley et al. 2019, 2021; Miller et al. 2019, 2021; Choudhury et al. 2024; Dittmann et al. 2024; Salmi et al. 2024; Vinciguerra et al. 2024).

Accreting millisecond pulsars (AMSPs; Patruno & Watts 2021; Di Salvo & Sanna 2022) represent an intriguing alternative. During accretion outbursts, they attain an X-ray luminosity of $L_{\rm X} \simeq 10^{36}$–10^{37} erg s^{-1}, i.e. 5–6 orders of magnitude brighter than rotation-powered MSPs. The degeneracy between M and $R_{\rm eq}$ and the spot geometrical and spectral parameters (see, e.g., Viironen & Poutanen 2004) prevented to get meaningful constraints from the data taken with, e.g., the Rossi X-ray Timing Explorer (M =1.2–1.6 $M_\odot$, $R_{\rm eq}$ =6–13 km by Poutanen & Gierliński 2003; M =0.8–1.7$M_\odot$, $R_{\rm eq}$ =5–13 km by Morsink & Leahy 2011). However, Salmi et al. (2018) showed that if i and θ were known a priori with an accuracy of a few degrees, those data would have allowed measurements with a relative uncertainty comparable to or slightly smaller than that for rotation-powered MSPs.

X-ray polarimetry might provide key information on the geometrical parameters of the spots. Soft photons from the NS surface are up-scattered by hot electrons in the accretion shock (Poutanen & Gierliński 2003) achieving polarization degree (PD) from a few per cent up to 10–20% (Nagirner & Poutanen 1994; Viironen & Poutanen 2004; Salmi et al. 2021; Bobrikova et al. 2023). The magnetic field strength of AMSPs (10^8–10^9 G) is too weak to affect X-ray photon polarization. As a result, the polarization vector of the X-rays emitted from the accretion shock is expected to lie either in the meridional plane, formed by the photon momentum and the normal to the surface, or perpendicular to it. As the NS rotates, the polarization angle (PA) should thus swing as a function of the pulsar spin phase in accordance with the rotating vector model (RVM; Radhakrishnan & Cooke 1969; Meszaros et al. 1988). In AMSPs, the relativistic motion of the emission regions causes additional rotation of the polarization plane (Poutanen 2020); also the oblate shape of a quickly rotating NS has to be accounted for (Loktev et al. 2020).

Here, we report on the discovery of polarized X-ray emission from the AMSP SRGA J144459.2−604207 (SRGA J1444 in the following) by the Imaging X-ray Polarimetry Explorer (IXPE; Weisskopf et al. 2022) in the context of a campaign which included also NICER, XMM-Newton, and NuSTAR observations. Discovered in outburst on 2024 February 21 by the *Mikhail Pavlinsky* ART-XC telescope on-board the Spectrum-Roentgen-Gamma observatory (Molkov et al. 2024) at a relatively bright 4–12 keV X-ray flux of 2×10^{-9} erg s^{-1} cm^{-2} (see Figure 1), SRGA J1444 showed coherent pulsations at 447.9 Hz first detected by NICER, coming from a NS in a 5.2 h orbit around a donor with a mass in the range 0.2–0.7 $M_\odot$ (Ng et al. 2024). SRGA J1444 also showed type-I X-ray bursts (Mariani et al. 2024) quite regularly, with a recurrence time increasing from 1.6 to 2.2 h as the X-ray flux was observed to decrease (Molkov et al. 2024). No optical counterpart could be identified (Baglio et al. 2024) at the most accurate X-ray position obtained with High Resolution Camera observations on board the Chandra observatory (Illiano et al. 2024), most likely due to the extinction of $A_{\rm V} \simeq 7$ mag (estimated[1] using the maps of

[1] see the tool available at http://astro.uni-tuebingen.de/nh3d/nhtool

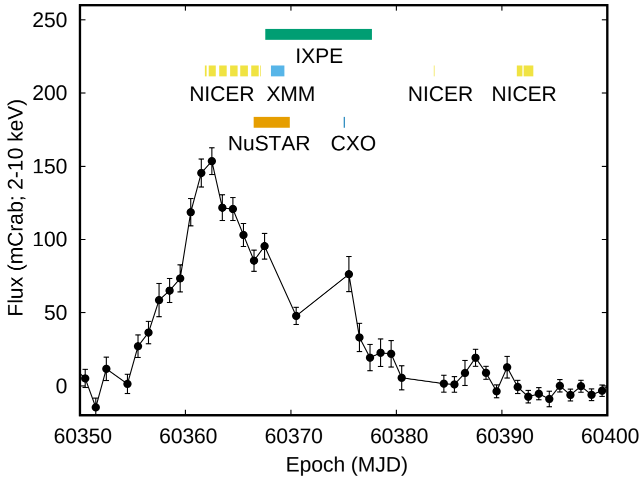

Figure 1. Light curve of the 2024 outburst of SRGA J1444 observed by MAXI (Matsuoka et al. 2009). We converted 2–20 keV observed count rates into 2–10 keV flux values assuming that the spectrum is described by a power law with a photon index $\Gamma = 1.9$ absorbed by an equivalent hydrogen column of $N_{\rm H} = 2.9\times10^{22}$ cm^{-2} (Ng et al. 2024). Horizontal bars indicate the time intervals covered by observations of the instruments discussed in this paper.

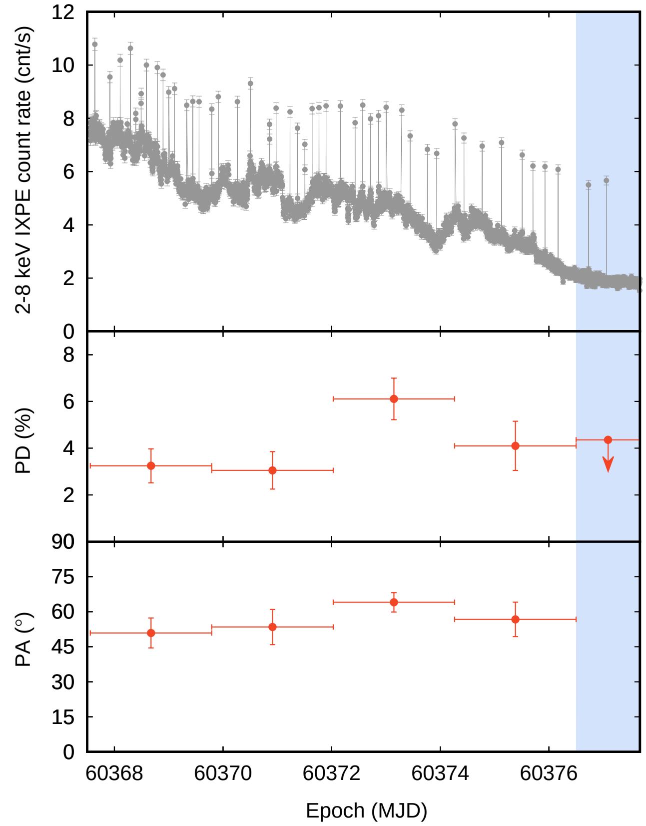

Figure 2. IXPE 2–8 keV light curve in 200 s time bins (top panel). Type-I X-ray bursts are easily recognized. PD (middle panel) and PA (bottom panel) measured in the 3–6 keV band and evaluated over $\sim$ 2 d-long intervals. The blue shaded region indicates the interval after the pulse amplitude increase observed at MJD 60376.5 in which a 90% c.l. upper limit on the PD is reported.

Doroshenko 2024, at a distance of 8 kpc) in that direction. Russell et al. (2024) reported a radio counterpart with a flux density of ~ 200 μJy at 5.5 GHz and a flat spectral shape, consistent with a compact jet or discrete ejecta.

2. OBSERVATIONS

Table 1 lists the observations analyzed in this paper, using HEASOFT package version 6.33.2. IXPE started observing SRGA J1444 less than a week after the first detection of the source, in response to the trigger of the GO program 03250101 (PI: A. Papitto). Observations lasted ~10 days with visibility gaps giving a duty cycle exceeding 60 per cent. We used the `pcube` algorithm in the `xpbin` tool of the IXPEOBSSIM package version 30.6.4 (Baldini et al. 2022), along with the IXPE CALDB released on 2024 February 28, to extract polarimetric information using the formalism from Kislat et al. (2015). We selected source photons from a circular region with a radius of 100″ centered at the source position. We use the unweighted analysis implemented in IXPEOBSSIM (Di Marco et al. 2022) to measure the Stokes parameters (I, Q, U). Figure 2 shows the 2–8 keV IXPE count rate, the polarization degree PD$=\sqrt{q^2+u^2}$ and angle PA$=\frac{1}{2}\arctan(u/q)$ measured in the 3–6 keV band, where $q = Q/I$ and $u = U/I$. As the source count rate is relatively high (~2–8 count s^{-1}), the background contributes at most 5% of the total rate and we did not subtract it following the recommendation of Di Marco et al. (2023). For the IXPE spectral analysis, we used the response matrices `20240101_alpha075` present in the CALDB, computed ancillary response files using `ixpecalcarf` weighting the Stokes parameters following the analysis presented by Di Marco et al. (2022) and binned the I spectra to have at least 30 counts per bin. To ensure statistics high enough for a spectro-polarimetric analysis, we binned data to a constant resolution of 200 eV.

Ng et al. (2024) reported the analysis of NICER observations during the first three days of the outburst using publicly available data. Here, we also include data taken afterwards in the GO program ID 663908 (PI: Papitto). Visibility constraints and high background prevented NICER to collect data simultaneously with the IXPE (see Figure 1). The monitoring briefly resumed on 2024 March 14 and more regularly after March 21, when

Table 1. Observations analyzed in this paper.

Observatory	Obs. ID	Start date (MJD)	End Date (MJD)	Instrument	Exposure (s)	Energy band (keV)
IXPE	03250101	60367.556	60377.676	DU1	552930	2–8
				DU2	553541	
				DU3	554066	
NICER	620419	60361.831	60363.908	XTI	9536	0.3–10
	663908	60364.219	60392.971		24805	
NuSTAR	80901307002	60366.459	60369.883	FPMA	157675	3–79
				FPMB	157440	
XMM-Newton	0923171501	60368.102	60369.376	EPIC-pn	110077	0.3–10

the source count rate had already decreased close to the background value. We reduced the observations using calibration version XTI20240206 and the same filtering criteria adopted by Ng et al. (2024), retaining photons with energy ranging between 0.3 and 10 keV for a pulse timing analysis.

The EPIC-pn telescope on-board XMM-Newton observed SRGA J1444 uninterruptedly for ∼110 ks. We retained 0.3–10 keV source photons extracted from a 21 pixel-wide stripe (equivalent to 86.″1) around the position of the pulsar to perform a pulse timing analysis.

NuSTAR provided the longest overlap with IXPE data starting on 2024 February 26. We reduced the data using the calibration version INDX20240325, which includes the fine clock correction file ver. 179. A circular region with a wide radius of 140″ was adopted to extract source photons in the 3–79 keV band.

The times of arrival of the photons recorded by all the instruments were transformed into the inertial reference frame centred at the Solar System barycenter using the Chandra coordinates reported by Illiano et al. (2024), R.A.= $14^{\rm h}\ 44^{\rm m}\ 58^{\rm s}.94$, Dec = $-60^\circ 41' 55.''3$ (J2000) and the DE 405 ephemeris. We detected 52, 5, 13 and 23 type-I X-ray bursts during IXPE, NICER, XMM-Newton and NuSTAR exposures, respectively. When analysing the *persistent* emission, we discarded intervals between 5-s before and 60-s after the onset of each burst.

3. RESULTS

3.1. *X-ray pulse timing*

We used the pulsar timing solutions based on the first few days of NICER observations (Ng et al. 2024) to correct the arrival time of X-ray photons for the light travel time delays due to the pulsar orbit. We used two harmonic components to model the pulse profiles obtained by folding data taken in ∼500 s-long intervals and sampled by 16 phase bins. Table 2 shows the timing solutions based on the observed evolution of the phase computed over the fundamental harmonic for the various instruments considered here, plotted in Fig. 3 with the best-fitting linear trend). We attribute the residual random phase variability by ∼0.05–0.1 cycles to pulse timing noise, as observed from other AMSPs with an even larger magnitude (Patruno & Watts 2021; Di Salvo & Sanna 2022). The two values of the pulse phase measured by NICER at MJD 60384, after an interruption of the monitoring due to visibility constraints, line up with the trend observed earlier and allow us to put a tight upper limit on the spin frequency derivative ($\dot{\nu} < 1.2\times10^{-13}$ Hz s^{-1}). However, we caution that such an alignment could be fortuitous, as the pulse phase of AMSPs often shows erratic variability, especially in the late stages of an outburst (see, e.g. Illiano et al. 2023).

We used these ephemerides to fold 5 ks-long intervals of IXPE data and recover the pulsed signal notwithstanding the lower counting statistics. Figure 4 shows the fractional amplitude and phase of the fundamental harmonic observed by IXPE. An increase of the amplitude from ∼ 4 to 15% is observed after MJD 60376.5.

The frequencies measured by NICER and NuSTAR are compatible within the errors ($\delta\nu/\nu \simeq 2\times10^{-10}$). On the other hand, IXPE and XMM-Newton show a frequency difference of $\delta\nu/\nu \simeq 0.6\times10^{-9}$ and 2×10^{-9} with respect to the NICER measurement, respectively. The latter is compatible with the value quoted in the latest calibration technical note for the XMM-Newton clock relative time accuracy[2] ($\delta\nu/\nu \simeq 10^{-8}$). The pulse phase recorded by NuSTAR and IXPE at epoch T_0 precedes those observed by NICER by 0.07–0.1 cycles. The NuSTAR shift can be understood in terms of the dependence of the pulse phase on energy already noticed by

[2] https://xmmweb.esac.esa.int/docs/documents/CAL-TN-0018.pdf

Table 2. Pulse phase timing solutions of SRGA J1444.

	NICER	XMM-Newton	NuSTAR	IXPE
Interval (MJD)	60361.837–60383.544	60368.106–60369.374	60366.465–60369.881	60367.615–60377.619
$\phi(T_0)$	0.47(1)	0.500(7)	0.396(2)	0.37(1)
$\nu(T_0)$ (Hz)	447.871561115(24)	447.87156196(24)	447.87156122(17)	447.87156138(8)
$\dot{\nu}$ (Hz s^{-1})	$< 1.2 \times 10^{-13}$	$< 7.0 \times 10^{-12}$	$< 7.4 \times 10^{-13}$	$< 3.0 \times 10^{-13}$
$a_1 \sin i/c$ (lt-s)	0.65052(2)	0.650491(5)	0.650494(4)	0.650486(13)
$P_{\rm orb}$ (s)	18803.65(1)	18803.65(1)	18803.690(4)	18803.665(4)
$T_{\rm asc}$ (MJD)	60361.641306(3)	60361.641305(6)	60361.641291(2)	60361.641310(5)
e	$< 9 \times 10^{-5}$	$< 9 \times 10^{-5}$	$< 3 \times 10^{-5}$	$< 1.0 \times 10^{-4}$
χ^2 (d.o.f.)	93.0 (53)	368.5 (212)	713.0 (378)	121.3 (53)

NOTE—All the solutions presented in the table were obtained by folding data around $\nu_{\rm fold} = 447.87156116029$ Hz with a reference epoch MJD 60361.8. To facilitate the comparison, the frequency estimates were evaluated at T_0 =MJD 60368.0. All the epochs reported here are given in the Barycentric Dynamical Time (TDB) system. Uncertainties at the 1σ confidence level are reported in parentheses. Upper limits are given at a 90% confidence level.

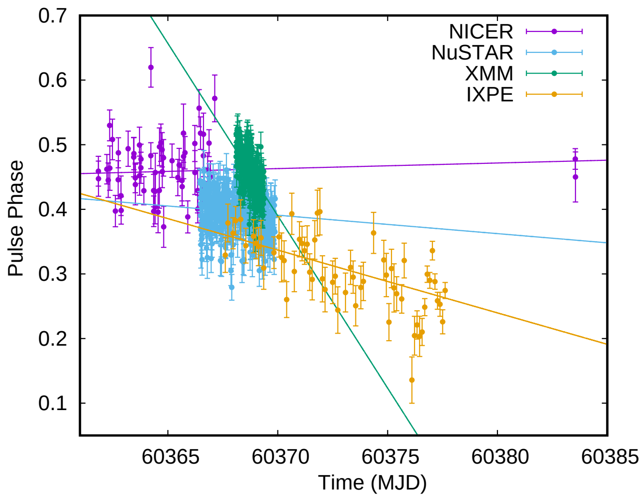

Figure 3. Pulse phase computed over the first harmonic of the pulses observed by NICER (magenta), NuSTAR (light blue), XMM-Newton (green) and IXPE (yellow) by folding 500 s-long intervals (5 ks for IXPE) around $\nu_{\rm fold}$ (see Table 2) with a reference epoch 60361.8 MJD. Solid lines mark the best-fit linear trends.

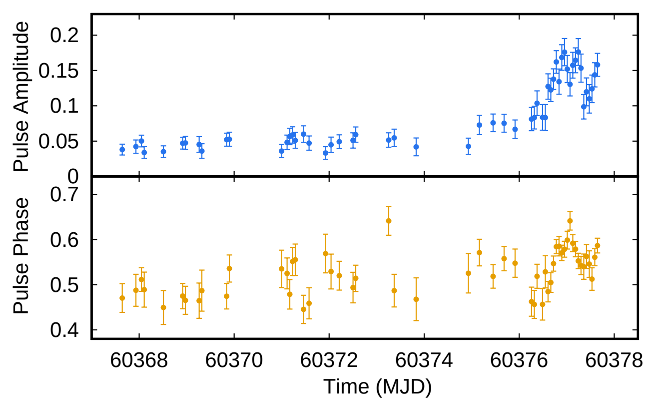

Figure 4. Pulse fractional amplitude and phase of the first harmonic component used to model the pulse profile obtained by folding IXPE data into 5 ks-long interval around the timing solution reported in the rightmost column of Table 2.

SRG/ART-XC (Molkov et al. 2024); the reason for the IXPE mismatch is less clear and will be addressed in a future paper. For consistency, the phase-resolved analysis presented in Sect. 3.3 is based on the IXPE timing solution, even if slightly less accurate.

3.2. *Polarized X-ray emission*

Figure 5 shows the average normalized Stokes parameters observed during the *persistent* emission by the three IXPE detector units. The average Stokes parameters are $q = -1.1 \pm 0.4\%$ and $u = 2.0 \pm 0.4\%$, which translate into an average PD of 2.3±0.4%, and an angle of PA 59°±6° (measured East of North, errors are quoted at the 1 σ c.l. unless differently specified; see Fig. 5). The probability of detecting such values of the normalized Stokes parameters from noise fluctuations is 1.1×10^{-7} (corresponding to a 5.3 σ c.l.). Figure 6 show the results of an energy-resolved analysis. Polarized emission is detected at the highest statistical significance in the 3–6 keV energy range with an average $\mathrm{PD}_{3-6} = 4.0\% \pm 0.5\%$ and $\mathrm{PA}_{3-6} = 57° \pm 3°$. Between 2 and 3 keV, the PD is not significant (0.7% ± 0.6%) with an upper limit at 90% confidence level of $\mathrm{PD}_{2-3} < 2.0\%$. Above 6 keV, the 5% upper limit on the PD becomes larger than both PD_{3-6} and the minimum detectable polarization at 99% confidence level in the 3–6 keV band (MDP_{99}=1.4%). We did not detect any significant variation or rotation of the 3–6 keV polarization vector over 2 d-long intervals, even though the PD slightly increases halfway through the observation (see bottom panels of Figure 2).

Similar to Ng et al. (2024), we used the sum of a black-body (`bbodyrad` in XSPEC) and thermal Comptonization (`nthcomp`) to satisfactorily model ($\chi^2 = 483.9$ for 441 d.o.f.) the 2–8 keV IXPE energy spectrum. We modelled absorption with the Tuebingen-Boulder model (Wilms et al. 2000) with the absorption column fixed to $N_{\rm H} = 2.9 \times 10^{22}$ cm^{-2} and quote uncertainties on the spectral parameters at 90% c.l. The thermal component has a temperature of $kT_{\rm bb} = 0.52 \pm 0.01$ keV and an apparent size of $R_{\rm bb} = (14.0 \pm 0.5)d_8$ km, where d_8 is the distance to the source in units of 8 kpc. Comptonization is described by an asymptotic power law with index $\Gamma = 1.70 \pm 0.03$ and a soft photon input with temperature < 0.15 keV. The electron temperature was fixed at a value beyond the IXPE bandpass $kT_{\rm e} = 15$ keV. The Comptonization component accounts for $\sim$ 95% of the 2–8 keV observed flux of $(5.6 \pm 0.1) \times 10^{-10}$ erg s^{-1} cm^{-2}. Spectral analysis of the NICER observation (Obs. ID 6639080103) performed $\sim$12 h before the start of the IXPE coverage indicates a smaller black-body size ($kT_{\rm bb} = 0.68 \pm 0.05$ keV; $R_{\rm bb} = (5.7 \pm 1.0)d_8$ km) and a steeper slope of the Comptonized emission ($\Gamma = 1.90 \pm 0.01$).

The decrease of the PD below 3 keV, i.e. where the soft thermal component gives its highest contribution to the 2–8 keV spectrum, motivated us to perform a spectro-polarimetric analysis. By fitting the spectra of the three Stokes parameters with a constant polarization component to multiply the model presented above, `tbabs*(bbodyrad+nthcomp)*polconst`, gave PD=2.6%±0.5% and PA=59°±6° with a χ^2/d.o.f. of 340/257, compatible with the `pcube` results. By using separate constant polarization for the two spectral components gave a slight improvement of the fit χ^2/d.o.f.=328/255 with a `bbodyrad` component polarized with the PD=8% ± 5% at PA=−43° ± 19° and the `nthcomp` with the PD=4.6% ± 1.1% and PA=55° ± 7°.

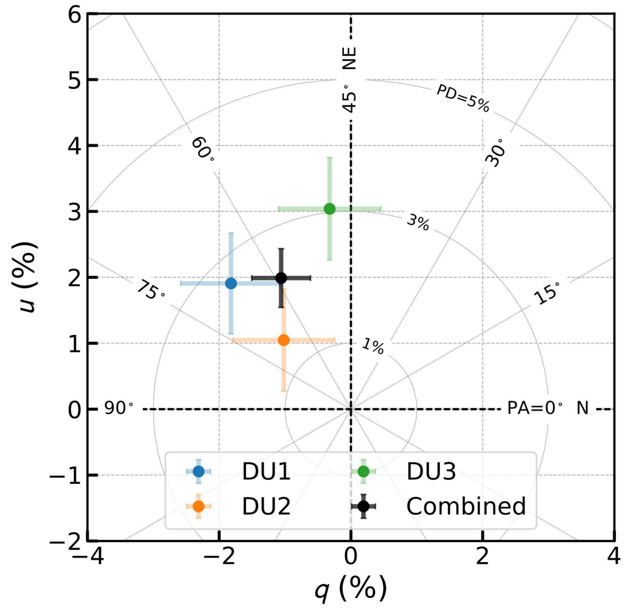

Figure 5. Average normalized Stokes parameters observed during the 2–8 keV *persistent* emission for the single IXPE DUs and for the sum.

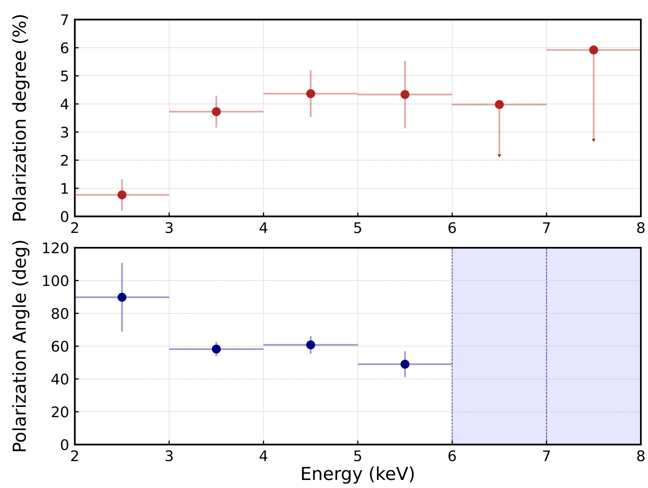

Figure 6. PD (top) and PA (bottom) as a function of energy. Above 6 keV, polarization is compatible with zero and we report upper limits at 90% c.l., while the PA is unconstrained.

3.3. *Phase-resolved variability of the polarized X-rays*

To perform a phase-resolved analysis of the polarimetric properties of SRGA J1444, we considered IXPE data corrected with the orbital parameters listed in Table 2. We used the `pcube` algorithm to evaluate in $n = 16$ phase bins the Stokes parameters Q and U, which are expected to be normally distributed (González-Caniulef et al. 2023; Suleimanov et al. 2023). We restricted the analysis to the 3–6 keV energy band in order to maximize the strength of the polarized signal. We used the `pcube` algorithm without acceptance corrections to measure the Stokes parameters in counts per second.

From top to bottom, Figure 7 shows the phase-resolved Stokes parameters, the PD and the PA observed before the pulse amplitude increase which occurred at MJD 60376.5. The Stokes parameters Q and U did not show significant variability. A fit with a constant func-

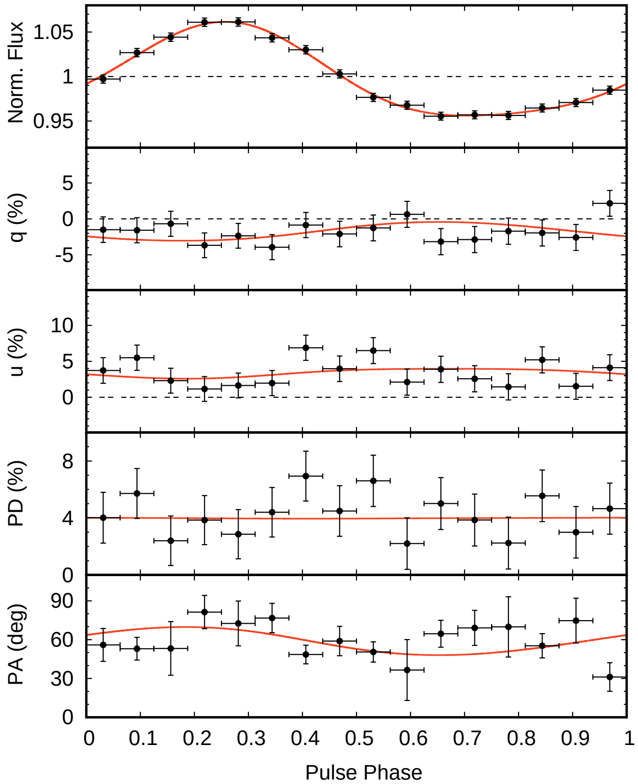

Figure 7. From top to bottom: total flux normalized to the average, normalized Stokes parameters $q = Q/I$ and $u = U/I$, the PD and PA observed by IXPE during the interval MJD 60367.6–60376.5, as a function of the spin phase. The solid red line indicates the model obtained fitting the absolute Stokes parameters assuming two point-like spots and the parameters listed in text.

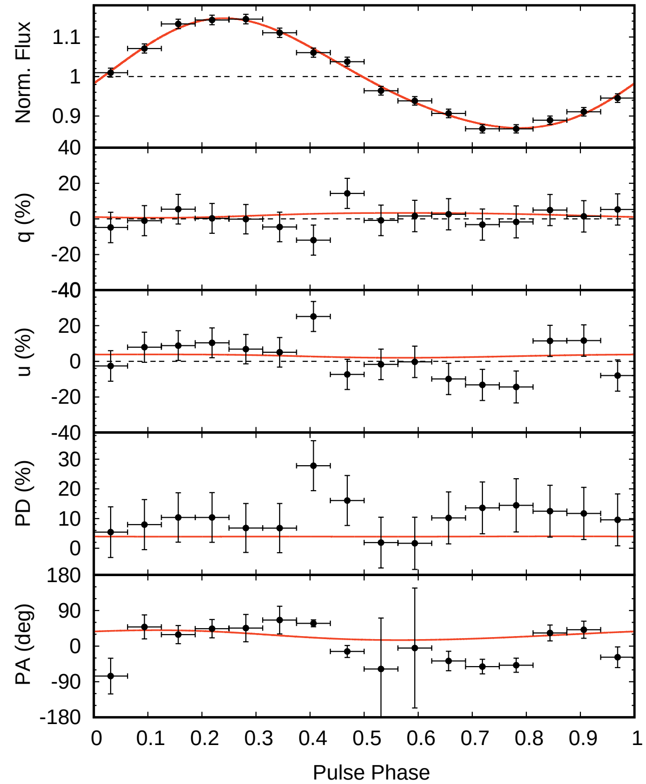

Figure 8. Same as Fig. 7 but for the interval MJD 60376.5–60377.7 only.

tion gave a χ^2 of 16.6 and 15.6 for 15 d.o.f., respectively, with average values of $q = Q/I = -1.6\% \pm 0.5\%$ and $u = U/I = 3.5\% \pm 0.4\%$.

We also analyzed separately data taken after the pulse amplitude increase which occurred at MJD 60376.5 (see Figure 8). Fitting with a constant gives $q' = 0.5\% \pm 1.4\%$ and $u' = 2.4\% \pm 2.7\%$ for $\chi^2 = 10.2$ and 18.7 for 15 d.o.f.. Both Stokes parameters are compatible with zero within the uncertainties, even though the value of u' measured at phase 0.4 significantly deviated from the trend, leading to an increase of the PD up to $\sim 30\%$.

We also measured the Stokes parameters over 15 orbital phase bins to search for orbital variability of the polarization properties but found none significant. Constant values of Q and U modeled well the dependence of these values on the orbital phase ($\chi^2 = 9.1$ and 12.5 for 14 d.o.f., respectively).

4. TYPE-I X-RAY BURSTS

During the observations reported here, IXPE detected 52 type-I X-ray bursts which shared similar properties (see the inset of Figure 9 for an example). The sample of peak count rates had an average of $38.7\,\mathrm{cnt\,s^{-1}}$ and a standard deviation of $2.9\,\mathrm{cnt\,s^{-1}}$. After subtracting the persistent emission, the distribution of the fluence of the observed bursts had an average of 649 cnt with a standard deviation of 40; the fluence of the different bursts was very similar and only slightly increased for bursts occurring when the persistent count rate had decreased below $3\,\mathrm{cnt\,s^{-1}}$. The relatively low number of counts observed by IXPE prevented us from performing a time-resolved spectral analysis of the single bursts. By stacking all the observed bursts, and fitting the observed spectra with the sum of a thermal component and the two-component model used to fit the persistent spectrum (see Sec. 3.2), we get $\langle kT_{\rm burst}\rangle = 1.83 \pm 0.05$ keV and $R_{\rm burst} = (6.2 \pm 0.2) d_8$ km. Defining the burst duration as $\tau = \mathcal{F}/F_{\rm peak}$, and neglecting variations of the spectrum throughout the burst, gives $\tau = 16.8 \pm 1.6$ s. Figure 9 shows the recurrence times $\Delta t_{\rm rec}$ between the observed bursts[3] as a function of the average persistent count rate C measured during the longest possible con-

[3] Consecutive bursts without data gaps could not be observed in IXPE data, but the uninterrupted XMM coverage allowed us to define the recurrence time unambiguously.

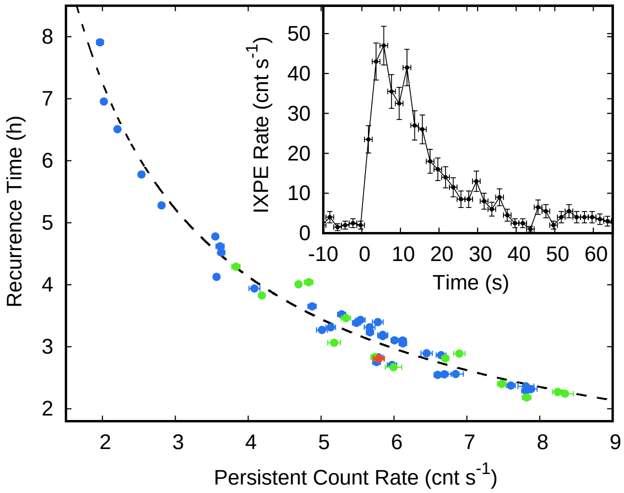

Figure 9. Recurrence time of the type-I X-ray bursts observed by IXPE evaluated as the interval between consecutive bursts scaled by a factor 1 (blue points), 2 (green) and 3 (red) as a function of the persistent count rate observed before the burst C. The dashed line shows the relation $\Delta t_{\rm rec} = KC^{-0.8}$ with $K = 12.75$ h. The inset shows the profile of the burst observed starting at MJD 60377.05969.

tiguous interval before the burst. For 14 bursts, we scaled the time elapsed since the previous burst by a factor of 2 as the immediately preceding burst was likely missed due to interruption in the IXPE coverage (green points in Figure 9). For one burst (red point), we used a scaling factor of 3.

To search for a polarized signal during the X-ray bursts, we stacked the emission observed during all the events, retaining 32 s after the onset of each of the bursts for a total exposure of 1664 s. We measured $q_{\rm b} = Q_{\rm b}/I_{\rm b} = -0.8\% \pm 3.3\%$ and $u_{\rm b} = U_{\rm b}/I_{\rm b} = 2.8\% \pm 3.3\%$, resulting in an upper limit on the PD of the sum of the burst and the persistent emission of $PD_{\rm UL} = 7.2\%$ (90% c.l.). We then subtracted the absolute Stokes vectors observed during the persistent emission after normalizing them to the exposure time of 1664 s over which the burst emission was integrated, summing in quadrature the uncertainties, and obtained normalized and *background* subtracted Stokes parameters $\tilde{q}_{\rm b} = -0.7\% \pm 3.9\%$ and $\tilde{u}_{\rm b} = 3.0\% \pm 3.9\%$, corresponding to an upper limit on the PD of 8.5% (90% c.l.). Such an upper limit is larger than $PD_{\rm UL}$ by a factor $1 + r \simeq 1.2$, where r is the ratio between the burst (only) and the persistent flux.

5. DISCUSSION

5.1. *Average polarization properties*

For the first time, IXPE observations of SRGA J1444 allowed us to significantly detect polarization from an AMSP with an average 2–8 keV degree of $2.3\% \pm 0.4\%$. Such a value increases to $4.0\% \pm 0.5\%$ if the analysis is restricted to the 3–6 keV energy band. Comptonization by hot ($kT_{\rm e}$ ∼20–60 keV) electrons in slabs of moderate optical depth (τ ≈1–2) located above hot spots ($kT_{\rm bb} \sim 1$ keV) on the NS surface accounts for more than 90% of the emission in the IXPE bandpass of AMSPs such as SRGA J1444 (Poutanen 2006) and represents the most natural explanation of the polarization we detected. Values of the PD as high as 10–20% were predicted by modelling the scattering in Thomson approximation (Viironen & Poutanen 2004; Salmi et al. 2021). However, the actual degree of polarization is a function of the physical properties of the scattering medium (Nagirner & Poutanen 1994). Recently, Bobrikova et al. (2023) applied the formalism for Compton scattering in a hot slab (Nagirner & Poutanen 1993; Poutanen & Svensson 1996) to describe the Stokes parameters as a function of energy and angle in terms of the electron temperature and optical depth of the slab and the seed photon temperature. They found values of the PD of a few per cent at the most, decreasing to values undetectable to IXPE at high (> 50 keV) electron temperatures. They concluded that chances for IXPE to detect polarization from an AMSP significantly increased for systems with a larger optical depth ($\tau > 2$) and lower electron temperature ($kT_{\rm e} < 30$ keV). Molkov et al. (2024) fitted the 4–30 keV ART-XC spectrum with Comptonization from a medium with $kT_{\rm e} \sim 25$ keV and $\tau \sim 3.2$ (evaluated from the photon index of $\Gamma = 1.8$ as in, e.g., Lightman & Zdziarski 1987). Preliminary fitting of the 3–79 keV NuSTAR spectrum (Malacaria et al., in prep.) suggests an even lower temperature ($kT_{\rm e} = 10.9^{+0.2}_{-0.1}$ keV) and higher optical depth ($\Gamma = 2.2 \pm 0.1$, $\tau = 4.0 \pm 0.3$). In the framework developed by Bobrikova et al. (2023), SRGA J1444 may thus present favorable spectral conditions to produce a relatively high degree of X-ray polarization compared to other AMSPs which might show even lower values. In addition, Bobrikova et al. (2023) showed that the observed polarization degree increased when an observer mostly sees the spot under high angles (i.e., $|i - \theta|$ close to π). Such a configuration is supported by the results presented in Sect. 5.2.

We detected a significant decrease in the PD below 3 keV. In the IXPE bandpass, that energy band is where the non-upscattered blackbody emission contributes the most to the total observed flux. However, even though these photons are not expected to be polarized, they only account for 5-10% of the total emission. As a result, the influence of such an unpolarized component at low energies does not readily explain the observed decrease of the PD. The analysis presented in Sec. 3.2 shows that, to explain the decrease of the total polarization, the polarization angle of the soft blackbody component (contributing to 7.7%±1.4% of the 2–3 keV emission, according to the NICER spectral analysis reported in Sect. 3.2) should differ by $\sim 90^\circ$ from the polarization angle compared of the Comptonization component . Yet, the relatively modest improvement of the fit description compared to a model with the same polarization properties for the two spectral components suggests that an intrinsic evolution of the polarization properties of the Compton scattered photons is a more likely explanation of the observed energy dependence. Bobrikova et al. (2023) predicted a swing by $\sim 90^\circ$ of the polarization vector of the Comptonized emission at an energy of $\simeq 5$ keV, only slightly higher than the turn-over energy of $\simeq 3$ keV we observed. A comprehensive analysis of the spectral properties of the source, including also XMM-Newton data, is in preparation.

5.2. *Phase-resolved analysis*

Assuming the accretion columns as the source of the polarized X-ray photons we observed, it is necessary to ask what spot geometrical configuration can explain at the same time the observed pulse profile and the non-significant phase-resolved variability of the Stokes parameters Q and U.

Unlike the case of highly magnetized, slowly rotating X-ray pulsars (Doroshenko et al. 2022; Tsygankov et al. 2022; Mushtukov et al. 2023; Marshall et al. 2022; Forsblom et al. 2023; Tsygankov et al. 2023; Malacaria et al. 2023; Doroshenko et al. 2023; Suleimanov et al. 2023; Poutanen et al. 2024; Forsblom et al. 2024), the polarization properties of AMSPs are defined by the geometry of the spots, relativistic effects (Poutanen 2020; Loktev et al. 2020), and possibly eclipses by the inner parts of the accretion disks (Poutanen et al. 2009; Ibragimov & Poutanen 2009). This does not allow us to use a simple rotating vector model to fit the observed phase-resolved PD and PA, but requires a fit of the total Stokes vector (I, Q, U) which is the sum of the Stokes vectors of the two spots.

The spots' Stokes parameters depend on how the total and polarized radiation vary with the spin phase, photon energy and zenith angle (Viironen & Poutanen 2004; Poutanen 2020; Salmi et al. 2021; Bobrikova et al. 2023). A modeling that includes an accurate description of all these effects is beyond the scope of this letter and will be presented elsewhere. Here, we draw considerations on the system's geometry by using the approximate formulae given by Poutanen & Beloborodov (2006) and Poutanen (2020) for the phase-resolved Stokes parameters. We assume two point-like spots on the surface of a rapidly rotating NS which emit X-rays with a power-law spectrum with $I(\alpha', E) = I_0(1 + h\cos\alpha')E^{-(\Gamma-1)}$. Here, $\Gamma = 1.9$ is the spectral photon index, α' is the zenith angle (i.e., the angle between the normal to the spot and emission direction) in the co-rotating frame and h is an anisotropy parameter ($h = 0$ for blackbody emission, $-1 < h < 0$ for a fan-beam pattern such that expected from Comptonization in a thin slab; Poutanen & Gierliński 2003). We used Eq. (20–22) of Poutanen & Beloborodov (2006) to determine the phase intervals in which the photons are visible to the observer and Eqs. (28–34) of the same paper to express the flux observed from each spot, $F_i(\phi_i + \phi_0, i, \theta_i, h)$ $(i = 1, 2)$ at a given binary inclination i and colatitude θ_i of the spot, and the resulting total flux $F_{\rm tot}(\phi) = N(F_1 + F_2)$. Here, N is a normalization constant, ϕ_0 is the spin phase of the primary spot at the folding reference epoch. We assumed the phase of the secondary spot to be $\phi_2 = \phi_1 + \pi$ and used the relativistic rotating vector model of Poutanen (2020) to express the phase-resolved Stokes parameters of each of the two spots (Eqs. 58–59), assuming that NF_i gives the observed flux and that their polarization degree $p_1 = p_2$ does not depend on energy and zenith angle. We then used (Eqs. 21–23) of the same paper to compute the total expected Stokes vector, $Q = Q_1 + Q_2$ and $U = U_1 + U_2$.

We fitted the phase-resolved Stokes parameters observed before the amplitude increase (see Figure 7) with our simple model fixing the NS mass and radius to $M = 1.4\,{\rm M}_\odot$ and $R_{\rm eq} = 12.5$ km (see Figure 7). The fit suggests a configuration with two visible spots as the fit χ^2 (38.8 for 41 d.o.f) improves compared to a fit with only one spot ($\chi^2 = 63.0$ for 42 d.o.f.; the probability of chance improvement is $\simeq 10^{-5}$ according to an F-test). A reasonably good fit can be obtained for any value of h ranging between 0 and -1; here we show the results obtained for a randomly chosen intermediate value of $h = -0.3$. We find a best-fit for $i = (74.1^{+5.8}_{-6.3})^\circ$, $\theta_1 = (11.8^{+2.5}_{-3.5})^\circ$, $\theta_2 = (172.6^{+2.0}_{-1.0})^\circ$, $\phi_0 = 0.57(4)$, $N = 6.90(6) \times 10^4$ cnt, $p_1 = 4.0\% \pm 2.0\%$ and $\chi_{\rm p} = 57.2^\circ \pm 0.5^\circ$, where the latter is the position angle of the pulsar angular momentum. We evaluated uncertainties at 1σ confidence level from the variation of the fit χ^2 for the number of interesting parameters measured ($\Delta\chi^2 = 8.15$ for 7 parameters Lampton et al. 1976). Such uncertainties have to be taken with caution, as they were obtained for fixed values of the NS mass, radius and emission anisotropy parameter. In addition, the large correlation between the parameters warrants a study of the posterior distribution of the parameters fitted using the likelihood function for I, Q and U, which will be presented in a forthcoming paper. The red line in Figure 7 marks the predicted model of the normalized Stokes parameters obtained for these parameters. Bottom panels of the same figure show the total PD= $\sqrt{q^2+u^2}$ and PA= $\chi_{\rm p}+\frac{1}{2}\tan^{-1}(u/q)$, respectively. The absence of significant variability with the pulse phase of the phase-resolved observed normalized Stokes parameters Q and U can be explained by two almost antipodal spots if their magnetic inclination is small. Yet, the observed roughly constant phase-resolved trend gives little information on the other parameters which are essentially set by the total pulse profile alone. Molkov et al. (2024) used a modeling similar to ours (even though they assumed extended spots) and found qualitatively similar results ($i=58°$ and $\theta_1=14°$, $\theta_2=\pi-\theta_1$). They modeled a pulse with a higher amplitude (9–12%) than ours (A_1 = 5.2%±0.1%) and a plateau close to the pulse minimum, which they interpreted in terms of occultation by the inner accretion disk extending down to ∼25 km. The flattening of the pulse profile observed by IXPE is less pronounced and partial occultation is not required to obtain qualitative modeling of the profile. Because the pulse profile Molkov et al. (2024) modeled was observed when the X-ray flux was roughly double that observed by IXPE, this could indicate a recession of the inner accretion disk at a decreasing mass accretion rate.

Interestingly, the increase of the pulsed fraction observed by IXPE after MJD 60376.5 to A_1 = 18.7%±0.8% (see Fig. 4 and Fig. 8) can be qualitatively explained assuming a fixed value of the binary inclination if the magnetic inclination of the two spots varies by $\delta\theta_1 \simeq -\delta\theta_2 \simeq 10°$, the longitude shifts by ∼20°and the polarized degree of each spot decreases to 2.0%±1.5%. The profile predicted using our model assumption and keeping the rest of the parameters to the values quoted above is plotted as a red line in Figure 8.

5.3. *Type-I X-ray bursts*

To our knowledge, the observations presented here are the first in which IXPE caught thermonuclear X-ray bursts from an accreting NS. The ∼10 d coverage of the outburst of SRGA J1444 allowed us to detect 52 bursts and stack them when searching for a polarized signal. The upper limit we put on the PD of the burst emission (8.5%) is higher than the maximum value estimated by Lapidus & Sunyaev (1985) assuming reflection of the burst emission by the accretion disk (3.7% for an inclination of 72°). With a recurrence time variable between ≃ 1.6 hr at the beginning of the outburst (Molkov et al. 2024) and ≃ 8 hr at the end of the IXPE observation presented here, SRGA J1444 was immediately recognized as a very prolific burster. The 11 Hz pulsar IGR J17480–2446 (which showed a recurrence time decreasing from ≃ 30 to ≃ 3 minutes; Motta et al. 2011; Chakraborty et al. 2011; Linares et al. 2012) and 4U 1636–536 (with a recurrence time of ≃ 30 minutes and even less energetic short recurrence time bursts; Beri et al. 2019) are similar cases. Among accreting MSPs, SAX J17498–2021 showed bursts between 1 and 2 hr (Li et al. 2018), IGR J17511–3057 between 7 and 21 hr (Falanga et al. 2011) and IGR J17498–2921 every 16–18 hr (Falanga et al. 2012), in all cases with a recurrence time increasing as the X-ray flux declined. The ≈ 15 s duration of the bursts seen from SRGA J1444 suggests that they ignite in a mixed H/He environment. Hot CNO cycle is expected to deplete the accreted hydrogen in $9.8(X/0.7)(Z/0.02)^{-1}$ hr, where H and Z are the hydrogen and metals abundances (see Galloway et al. 2022, and references therein). The range of observed recurrence times (< 8 hr) suggests that complete depletion of hydrogen could only be achieved if the H abundance is sub-solar. For bursts igniting in a mixed H/He environment, the burst ignition depth is not expected to depend much on the mass accretion rate $\dot{M}$ and the recurrence time scale should increase as $\Delta t \propto \dot{M}^{-1}$. Assuming that the IXPE count rate is a good tracer of the mass accretion rate, the observed dependence (see Fig. 9) is broadly compatible with such an expectation. Malacaria et al. (in prep.) will present a detailed analysis of the burst ignition process on this fast rotating pulsar allowed by the long and high duty cycle allowed by IXPE.

6. CONCLUSIONS

We presented the first X-ray polarimetric IXPE observation of an accreting millisecond pulsar in outburst, SRGA J1444, in the context of an observational campaign involving also NICER, NuSTAR and XMM-Newton observations. The main results are the following:

- The 2-8 keV emission is significantly polarized, with an average degree of $2.3\% \pm 0.4\%$ at an angle of $59° \pm 6°$ (East of North).
- We observed a significant change of the polarization properties with energies. The PD is maximum between 3 and 6 keV ($4.0\% \pm 0.5\%$) and decreases to < 2% (90% c.l.) in the 2–3 keV range.
- The pulse phase of SRGA J1444 is rather stable throughout the observations presented here, with an upper limit on the spin frequency derivative of $\dot{\nu} < 1.2 \times 10^{-13}$ Hz s^{-1}. During IXPE observations the pulse has an amplitude of ∼ 5%, before abruptly increasing to almost 20%, roughly one day before the end of the coverage.

- The observed phase-resolved Stokes parameters are compatible with a constant function. A simple approximate model of the Stokes vector expected from the sum of two almost antipodal spots on the NS surface reproduces the observed values for a binary inclination of $i = (74.1^{+5.8}_{-6.3})^\circ$ and relatively small magnetic inclination of the spots $\theta_1 = (11.8^{+2.5}_{-3.5})^\circ$, $\theta_2 = (172.6^{+2.0}_{-1.0})^\circ$. The little phase-resolved variability shown by the Stokes parameters, if any, prevented us from obtaining constraints on the NS mass and radius based on our simple modeling.

- IXPE observed 52 type-I X-ray bursts sharing similar properties (e.g. burst peak fluence, duration, fluence) with a recurrence time increasing as a function of the observed count rate, $\Delta t_{\rm rec} \propto C^{-0.8}$. After subtracting the persistent emission, the upper limit on the PD observed in the stacked burst emission is 8.5% (90% c.l.).

The first significant detection of polarization from an accreting millisecond pulsar confirms theoretical expectations and strengthens the prospects of using this technique to measure the geometrical parameters of accreting MSPs and obtain constraints on the mass and radius of the NS from pulse profile modeling. Future IXPE observations of accreting millisecond pulsars outbursts will hopefully detect a larger phase-resolved variability and enable more accurate determination than those allowed by the present dataset.

ACKNOWLEDGMENTS

We warmly thank the Directors and the Science Operations Team of IXPE, NICER, NuSTAR and XMM for promptly scheduling the observations reported here, as well as Anna Watts and Bas Dorsman for useful discussions.

NICER is a 0.2–12 keV X-ray telescope operating on the International Space Station, funded by NASA. The Imaging X-ray Polarimetry Explorer (IXPE) is a joint US and Italian mission. The US contribution is supported by the National Aeronautics and Space Administration (NASA) and led and managed by its Marshall Space Flight Center (MSFC), with industry partner Ball Aerospace (contract NNM15AA18C). The Italian contribution is supported by the Italian Space Agency (Agenzia Spaziale Italiana, ASI) through contract ASI-OHBI-2022-13-I.0, agreements ASI-INAF-2022-19-HH.0 and ASI-INFN-2017.13-H0, and its Space Science Data Center (SSDC) with agreements ASI-INAF-2022-14-HH.0 and ASI-INFN 2021-43-HH.0, and by the Istituto Nazionale di Astrofisica (INAF) and the Istituto Nazionale di Fisica Nucleare (INFN) in Italy. This research used data products provided by the IXPE Team (MSFC, SSDC, INAF, and INFN) and distributed with additional software tools by the High-Energy Astrophysics Science Archive Research Center (HEASARC), at NASA Goddard Space Flight Center (GSFC). The NuSTAR mission is a project led by the California Institute of Technology, managed by the Jet Propulsion Laboratory, and funded by the National Aeronautics and Space Administration. Data analysis was performed using the NuSTAR Data Analysis Software (NuSTARDAS), jointly developed by the ASI Science Data Center (SSDC, Italy) and the California Institute of Technology (USA). XMM-Newton is an ESA science mission with instruments and contributions directly funded by ESA Member States and NASA.

AP, GI, FA, RLP, CM and LS are supported by INAF (Research Grant "Uncovering the optical beat of the fastest magnetised neutron stars (FANS)") and the Italian Ministry of University and Research (MUR) (PRIN 2020, Grant 2020BRP57Z, "Gravitational and Electromagnetic-wave Sources in the Universe with current and next-generation detectors (GEMS)"). JP and VL thank the Academy of Finland grant 333112 and Minobrnauki grant 075-15-2024-647 for support. AB acknowledges support from the Finnish Cultural Foundation grant 00240328. MCB acknowledges support from the INAF-Astrofit fellowship. FCZ is supported by a Ramón y Cajal fellowship (grant agreement RYC2021-030888-I).

REFERENCES

Baglio, M. C., Russell, D. M., Saikia, P., et al. 2024, The Astronomer's Telegram, 16487, 1

Baldini, L., Bucciantini, N., Di Lalla, N., et al. 2022, SoftwareX, 19, 101194, doi: 10.1016/j.softx.2022.101194

Baym, G., Hatsuda, T., Kojo, T., et al. 2018, Reports on Progress in Physics, 81, 056902, doi: 10.1088/1361-6633/aaae14

Beri, A., Paul, B., Yadav, J. S., et al. 2019, MNRAS, 482, 4397, doi: 10.1093/mnras/sty2975

Bobrikova, A., Loktev, V., Salmi, T., & Poutanen, J. 2023, A&A, 678, A99, doi: 10.1051/0004-6361/202346833

Chakraborty, M., Bhattacharyya, S., & Mukherjee, A. 2011, MNRAS, 418, 490, doi: 10.1111/j.1365-2966.2011.19499.x

Choudhury, D., Salmi, T., Vinciguerra, S., et al. 2024, arXiv e-prints, arXiv:2407.06789, doi: 10.48550/arXiv.2407.06789

Di Marco, A., Costa, E., Muleri, F., et al. 2022, AJ, 163, 170, doi: 10.3847/1538-3881/ac51c9

Di Marco, A., Soffitta, P., Costa, E., et al. 2023, AJ, 165, 143, doi: 10.3847/1538-3881/acba0f

Di Salvo, T., & Sanna, A. 2022, in ASSL, Vol. 465, Millisecond Pulsars, ed. S. Bhattacharyya, A. Papitto, & D. Bhattacharya, 87–124, doi: 10.1007/978-3-030-85198-9_4

Dittmann, A. J., Miller, M. C., Lamb, F. K., et al. 2024, arXiv e-prints, arXiv:2406.14467, doi: 10.48550/arXiv.2406.14467

Doroshenko, V. 2024, arXiv e-prints, arXiv:2403.03127, doi: 10.48550/arXiv.2403.03127

Doroshenko, V., Poutanen, J., Tsygankov, S. S., et al. 2022, Nature Astronomy, 6, 1433, doi: 10.1038/s41550-022-01799-5

Doroshenko, V., Poutanen, J., Heyl, J., et al. 2023, A&A, 677, A57, doi: 10.1051/0004-6361/202347088

Falanga, M., Kuiper, L., Poutanen, J., et al. 2012, A&A, 545, A26, doi: 10.1051/0004-6361/201219582

—. 2011, A&A, 529, A68, doi: 10.1051/0004-6361/201016240

Forsblom, S. V., Poutanen, J., Tsygankov, S. S., et al. 2023, ApJL, 947, L20, doi: 10.3847/2041-8213/acc391

Forsblom, S. V., Tsygankov, S. S., Poutanen, J., et al. 2024, A&A, submitted, arXiv:2406.08988, doi: 10.48550/arXiv.2406.08988

Galloway, D. K., Johnston, Z., Goodwin, A., & He, C.-C. 2022, ApJS, 263, 30, doi: 10.3847/1538-4365/ac98c9

González-Caniulef, D., Caiazzo, I., & Heyl, J. 2023, MNRAS, 519, 5902, doi: 10.1093/mnras/stad033

Ibragimov, A., & Poutanen, J. 2009, MNRAS, 400, 492, doi: 10.1111/j.1365-2966.2009.15477.x

Illiano, G., Papitto, A., Sanna, A., et al. 2023, ApJL, 942, L40, doi: 10.3847/2041-8213/acad81

Illiano, G., Coti Zelati, F., Marino, A., et al. 2024, The Astronomer's Telegram, 16510, 1

Kislat, F., Clark, B., Beilicke, M., & Krawczynski, H. 2015, Astroparticle Physics, 68, 45, doi: 10.1016/j.astropartphys.2015.02.007

Lampton, M., Margon, B., & Bowyer, S. 1976, ApJ, 208, 177, doi: 10.1086/154592

Lapidus, I. I., & Sunyaev, R. A. 1985, MNRAS, 217, 291, doi: 10.1093/mnras/217.2.291

Lattimer, J. M., & Prakash, M. 2016, PhR, 621, 127, doi: 10.1016/j.physrep.2015.12.005

Li, Z., De Falco, V., Falanga, M., et al. 2018, A&A, 620, A114, doi: 10.1051/0004-6361/201833857

Lightman, A. P., & Zdziarski, A. A. 1987, ApJ, 319, 643, doi: 10.1086/165485

Linares, M., Altamirano, D., Chakrabarty, D., Cumming, A., & Keek, L. 2012, ApJ, 748, 82, doi: 10.1088/0004-637X/748/2/82

Lo, K. H., Miller, M. C., Bhattacharyya, S., & Lamb, F. K. 2013, ApJ, 776, 19, doi: 10.1088/0004-637X/776/1/19

Loktev, V., Salmi, T., Nättilä, J., & Poutanen, J. 2020, A&A, 643, A84, doi: 10.1051/0004-6361/202039134

Malacaria, C., Heyl, J., Doroshenko, V., et al. 2023, A&A, 675, A29, doi: 10.1051/0004-6361/202346581

Mariani, I., Motta, S., Baglio, M. C., et al. 2024, The Astronomer's Telegram, 16475, 1

Marshall, H. L., Ng, M., Rogantini, D., et al. 2022, ApJ, 940, 70, doi: 10.3847/1538-4357/ac98c2

Matsuoka, M., Kawasaki, K., Ueno, S., et al. 2009, PASJ, 61, 999, doi: 10.1093/pasj/61.5.999

Meszaros, P., Novick, R., Szentgyorgyi, A., Chanan, G. A., & Weisskopf, M. C. 1988, ApJ, 324, 1056, doi: 10.1086/165962

Miller, M. C., & Lamb, F. K. 2015, ApJ, 808, 31, doi: 10.1088/0004-637X/808/1/31

—. 2016, European Physical Journal A, 52, 63, doi: 10.1140/epja/i2016-16063-8

Miller, M. C., Lamb, F. K., Dittmann, A. J., et al. 2019, ApJL, 887, L24, doi: 10.3847/2041-8213/ab50c5

—. 2021, ApJL, 918, L28, doi: 10.3847/2041-8213/ac089b

Molkov, S. V., Lutovinov, A. A., Tsygankov, S. S., et al. 2024, A&A, submitted, arXiv:2404.19709, doi: 10.48550/arXiv.2404.19709

Morsink, S. M., & Leahy, D. A. 2011, ApJ, 726, 56, doi: 10.1088/0004-637X/726/1/56

Motta, S., D'Aì, A., Papitto, A., et al. 2011, MNRAS, 414, 1508, doi: 10.1111/j.1365-2966.2011.18483.x

Mushtukov, A. A., Tsygankov, S. S., Poutanen, J., et al. 2023, MNRAS, 524, 2004, doi: 10.1093/mnras/stad1961

Nagirner, D. I., & Poutanen, J. 1993, A&A, 275, 325

—. 1994, Astrophysics and Space Physics Reviews, 9, 1

Ng, M., Ray, P. S., Sanna, A., et al. 2024, ApJL, 968, L7, doi: 10.3847/2041-8213/ad4edb

Özel, F., & Freire, P. 2016, ARA&A, 54, 401, doi: 10.1146/annurev-astro-081915-023322

Patruno, A., & Watts, A. L. 2021, in ASSL, Vol. 461, Timing Neutron Stars: Pulsations, Oscillations and Explosions, ed. T. M. Belloni, M. Méndez, & C. Zhang, 143–208, doi: 10.1007/978-3-662-62110-3_4

Poutanen, J. 2006, Advances in Space Research, 38, 2697, doi: 10.1016/j.asr.2006.04.025

—. 2020, A&A, 641, A166, doi: 10.1051/0004-6361/202038689

Poutanen, J., & Beloborodov, A. M. 2006, MNRAS, 373, 836, doi: 10.1111/j.1365-2966.2006.11088.x

Poutanen, J., & Gierliński, M. 2003, MNRAS, 343, 1301, doi: 10.1046/j.1365-8711.2003.06773.x

Poutanen, J., Ibragimov, A., & Annala, M. 2009, ApJL, 706, L129, doi: 10.1088/0004-637X/706/1/L129

Poutanen, J., & Svensson, R. 1996, ApJ, 470, 249, doi: 10.1086/177865

Poutanen, J., Tsygankov, S. S., Doroshenko, V., et al. 2024, A&A, submitted, arXiv:2405.08107, doi: 10.48550/arXiv.2405.08107

Radhakrishnan, V., & Cooke, D. J. 1969, Astrophys. Lett., 3, 225

Riley, T. E., Watts, A. L., Bogdanov, S., et al. 2019, ApJL, 887, L21, doi: 10.3847/2041-8213/ab481c

Riley, T. E., Watts, A. L., Ray, P. S., et al. 2021, ApJL, 918, L27, doi: 10.3847/2041-8213/ac0a81

Russell, T. D., Carotenuto, F., van den Eijnden, J., et al. 2024, The Astronomer's Telegram, 16511, 1

Salmi, T., Loktev, V., Korsman, K., et al. 2021, A&A, 646, A23, doi: 10.1051/0004-6361/202039470

Salmi, T., Nättilä, J., & Poutanen, J. 2018, A&A, 618, A161, doi: 10.1051/0004-6361/201833348

Salmi, T., Choudhury, D., Kini, Y., et al. 2024, arXiv e-prints, arXiv:2406.14466, doi: 10.48550/arXiv.2406.14466

Suleimanov, V. F., Forsblom, S. V., Tsygankov, S. S., et al. 2023, A&A, 678, A119, doi: 10.1051/0004-6361/202346994

Tsygankov, S. S., Doroshenko, V., Poutanen, J., et al. 2022, ApJL, 941, L14, doi: 10.3847/2041-8213/aca486

Tsygankov, S. S., Doroshenko, V., Mushtukov, A. A., et al. 2023, A&A, 675, A48, doi: 10.1051/0004-6361/202346134

Viironen, K., & Poutanen, J. 2004, A&A, 426, 985, doi: 10.1051/0004-6361:20041084

Vinciguerra, S., Salmi, T., Watts, A. L., et al. 2024, ApJ, 961, 62, doi: 10.3847/1538-4357/acfb83

Watts, A. L., Andersson, N., Chakrabarty, D., et al. 2016, Reviews of Modern Physics, 88, 021001, doi: 10.1103/RevModPhys.88.021001

Weisskopf, M. C., Soffitta, P., Baldini, L., et al. 2022, JATIS, 8, 026002, doi: 10.1117/1.JATIS.8.2.026002

Wilms, J., Allen, A., & McCray, R. 2000, ApJ, 542, 914, doi: 10.1086/317016